DESIGN AND FABRICATION OF BROADBAND ANTI-REFLECTION COATINGS FOR THE M.A.E.S.T.R.O. SPECTROGRAPH

by

Candido Dionisio Pinto

A Dissertation Submitted to the Faculty of the

Materials Science and Engineering

In Partial Fulfillment of the Requirements
For the Degree of

Doctor of Philosophy

In the Graduate College

The University of Arizona

Fall 2003

Abstract

This dissertation contains describes the design and manufacturing techniques of antireflection coatings for the optical components of the MAESTRO spectrograph. It spawned from the need of a high-performance, robust and inexpensive anti-reflection (AR) coating for deep-space, faint object astronomical observations. We have created a new line of AR-filters, optimal for several different glass substrates, with a small number of layers, and simple to manufacture. The ease of mass-manufacture of the Coyote® coating is also illustrated here, as well as future directions for this research.

Table of Contents

TABLE OF CONTENTS—*Continued*

List of Figures

List of Tables

Chapter 1

INTRODUCTION

1.1 Earth-Based Astronomical Spectrographs

Imaging through a randomly inhomogeneous media imposes strong limitations on the resolution achieved by any earth-based optical system. Such is the case for terrestrial telescopes, where atmospheric turbulence limits the resolution of long-exposure astronomical images to approximately one arcsecond [1]. However, despite the recent success of space-based telescopes within the last decade, their cost has made the proliferation of such systems prohibitive.

As a result, a new generation of large, earth-based telescopes have been built in different locations around the globe, such as Keck (Hawaii), Gemini, VLT and Magellan (Chile) and the MMT in Arizona. Their large apertures make high-resolution optical spectroscopy of faint and distant objects possible for the first time [2].

Although increasing the angular resolution of terrestrial telescopes is still an open problem which demands the effort of many scientists and engineers working in different fields [3], high-resolution echelle spectrographs attached to larger terrestrial telescopes are useful to the study of the intergalactic medium and contribute significantly to our knowledge of evolutionary cosmology [2].

1.2 The M.A.E.S.T.R.O. Spectrograph

"MAESTRO" stands for Multiple Mirror Telescope Advanced Echelle Spectrograph. The Multiple Mirror Telescope has recently been converted to a single 6.5 m single primary mirror telescope [4], fabricated by the Steward Observatory Mirror Lab at the University of Arizona. The optical system for MAESTRO is depicted in Figure 1.1 below. It is a multi-configuration system, comprising of twenty-one zoom positions for different wavelengths. All elements shall be optimally AR-coated, with the exception of the calcium fluoride biconvex element at the center of the triplet, and the proximal surfaces of the outer two elements of the triplet. Those elements will be secured with Cargille 5610® laser oil, which will also act as index matching media between the glass surfaces, making the application of an AR-filter on these surfaces unnecessary.

MAESTRO is an F/3 instrument, located at the F/5 Cassegrain focus of the Multiple Mirror Telescope. The beam is converted onto an F/3 via injection optical elements, manufactured locally by Tucson Optical Research Corporation. Those elements are optimally coated with the Gila® (calcium fluoride substrates) and

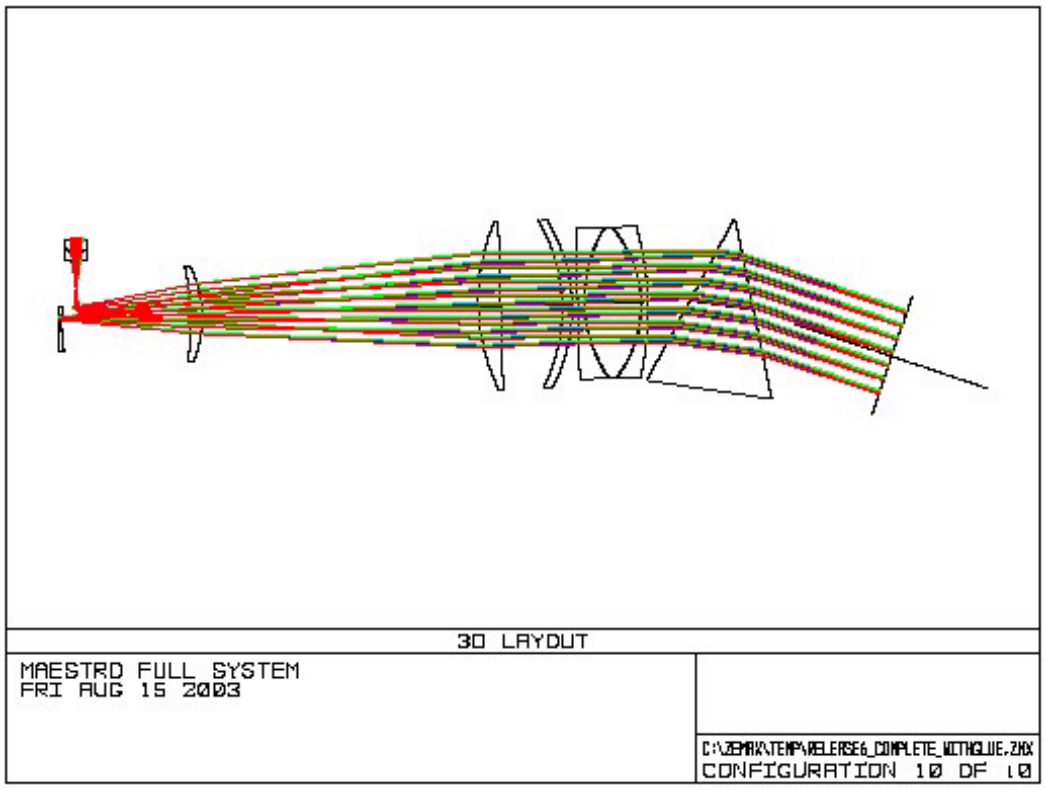

FIGURE 1.1. Full optical system layout for the MAESTRO Spectrograph.

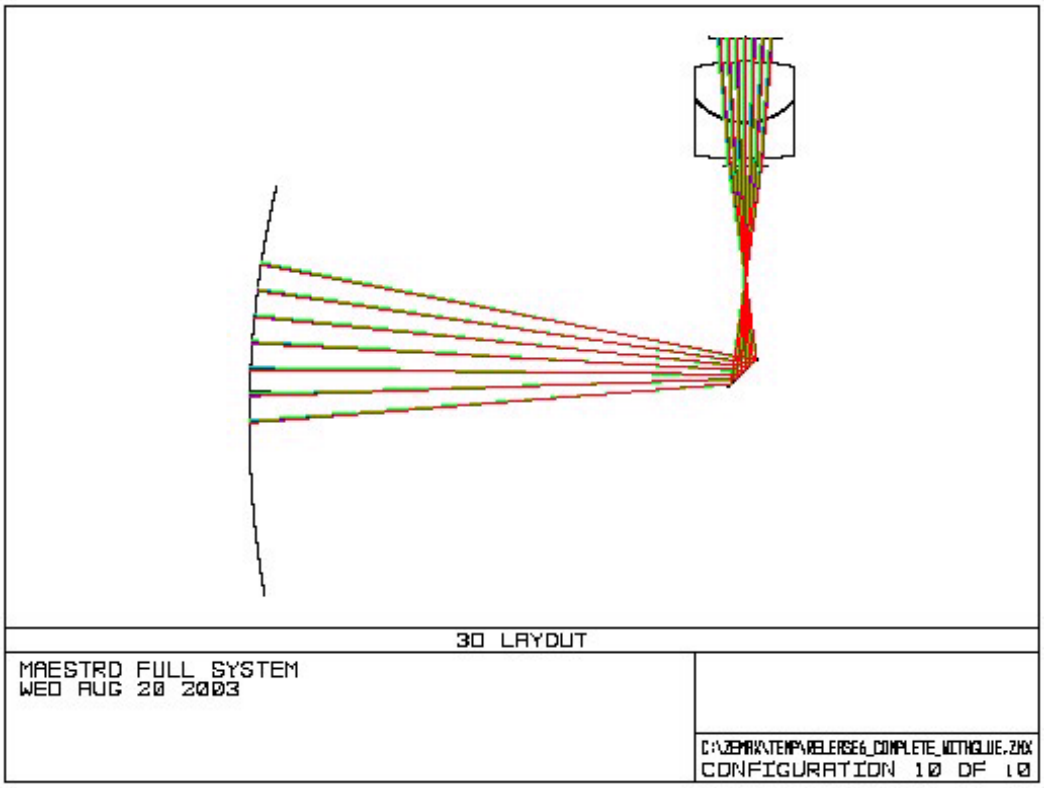

FIGURE 1.2. Detail of the injection optical subsystem in MAESTRO.

Coyote® (fused silica substrates) anti-reflection filters. The injection optical subsystem is shown below in Figure 1.2.

MAESTRO also has two dispersing elements: an AR-coated fused silica prism, and a custom Echelle grating, manufactured by Richardson Grating Labs, Inc. Its wavelength performance is optimal between 320 nm and 1100 nm, being effectively limited only by atmospheric transmission and silicon CCD performance. Detector performance is shown on Figure 1.3.

1.3 Outline of this Work

This dissertation describes my work at the Optical Sciences Center, Materials Science and Engineering dip-coating laboratory and Steward Observatory to design extremely broadband and robust anti-reflection coatings for different glass substrates. The optimal broadband AR-coating for astronomy is one with as much transmission as can be achieved, with a flat transmission curve, and resilient against temperature and humidity fluctuations caused by the environment.

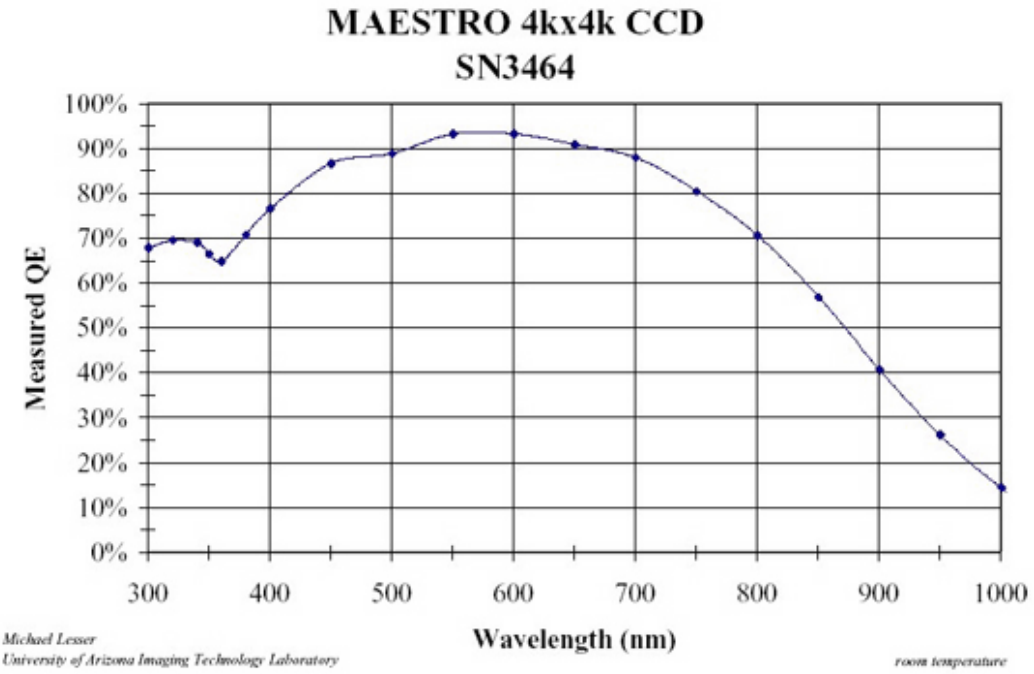

FIGURE 1.3. Measured Quantum Efficiency of CCD array custom-manufactured for MAESTRO Spectrograph.

I have made a summary of the required concepts and equations in order to approach the coating designs. We start with fundamentals of electromagnetic theory, going through the wave equation, time-harmonic fields, multiple-beam interference and basic coating design theory. All theoretical fundamentals necessary for the educated reader to understand interference filters are shown in Chapter 2.

In Chapter 3 design starting points and final prescriptions, along with their performance plots are shown. The process of choice of a moisture barrier is also illustrated, and we show that the search for a practical moisture barrier is still a work in progress.

The coating design for fused silica substrates is tested with real data in Chapter 4. We report the hybrid manufacturing technique, as well as resuls from environmental testing. Later, we deposit the Coyote® coating on 1 in diameter fused silica lenses and on the fused silica injection element and report on the results obtained. A comparison with current commercially available coatings is also done at the conclusion of this chapter.

Finally, in Chapter 5 several subjects are discussed. Among them are: possible solutions to the issue of depositing a hard coating layer on top of solgel, better potential choices for moisture and environmental barrier layers, and a proposed design for a long-lasting high-reflectance coating for telescope mirrors. Conclusions of this work are also given in Chapter 5, as well as future plans for controlled differential deposition and the design of a novel narrowband astronomical filter.

Chapter 2
THEORETICAL BACKGROUND

2.1 Fundamentals of Interference Filters

2.1.1 The Wave Equation

In linear, isotropic media, Maxwell's equations and their correspondent material equations are given by [5]:

$$\nabla \times \overrightarrow{H} - \frac{\partial \overrightarrow{D}}{\partial t} = \overrightarrow{j} \tag{2.1}$$

$$\nabla \times \overrightarrow{E} + \frac{\partial \overrightarrow{B}}{\partial t} = 0 \tag{2.2}$$

$$\nabla \cdot \overrightarrow{D} = \rho \tag{2.3}$$

$$\nabla \cdot \overrightarrow{B} = 0, \text{ where} \tag{2.4}$$

$$\overrightarrow{j} = \sigma \overrightarrow{E} \tag{2.5}$$

$$\overrightarrow{D} = \epsilon \overrightarrow{E} \tag{2.6}$$

$$\overrightarrow{B} = \mu \overrightarrow{H}. \tag{2.7}$$

and:

$$\epsilon = \epsilon_r \epsilon_0 \tag{2.8}$$

$$\mu = \mu_r \mu_0 \tag{2.9}$$

$$c = \frac{1}{\sqrt{\epsilon_0 \mu_0}} \tag{2.10}$$

defined as follows in the S.I. system of units:

$$c = 2.997925 \times 10^8 \frac{\text{m}}{\text{s}} \tag{2.11}$$

$$\mu_0 = 4\pi \times 10^{-7} \frac{\text{H}}{\text{m}} \tag{2.12}$$

$$\epsilon_0 = 8.8541853 \times 10^{-12} \frac{\text{F}}{\text{m}}. \tag{2.13}$$

In the absence of sources, Gauss's law 2.3 becomes:

$$\nabla \cdot \overrightarrow{D} = 0. \tag{2.14}$$

We can then take the curl of both sides of Faraday's law 2.2:

$$\nabla \times \left(\nabla \times \overrightarrow{E} \right) = -\frac{\partial}{\partial t} \left(\nabla \times \overrightarrow{B} \right) \tag{2.15}$$

and use the vector identity [5]:

$$\nabla \times \left(\nabla \times \overrightarrow{A} \right) = \nabla \left(\nabla \cdot \overrightarrow{A} \right) - \nabla^2 \overrightarrow{A} \tag{2.16}$$

substitute the right-hand side by the equality from Ampere's law 2.1 and find the well-known result:

$$\nabla^2 \overrightarrow{E} = \mu \left(\epsilon \frac{\partial^2 \overrightarrow{E}}{\partial t^2} + \sigma \frac{\partial \overrightarrow{E}}{\partial t} \right). \tag{2.17}$$

If the propagation medium is a dielectric (such as air, vacuum or glass), the electric conductivity $\sigma = 0$ giving the result:

$$\nabla^2 \overrightarrow{E} = \mu\epsilon \frac{\partial^2 \overrightarrow{E}}{\partial t^2}. \tag{2.18}$$

2.1.2 Multiple-Beam Interference

Let us consider the parallel film shown below on Figure 2.1, following Eugene Hecht's text [6]. Let the thickness of the dielectric film be d and θ_t the angle of refraction of the transmitted beam, inside the film, and λ_0 the vacuum wavelength of the incident light field. We can then write that the total reflected amplitude at point P is given by the sum of scalar amplitudes, as such:

$$E_r = E_0 \left[r + tt'r' \exp\left(i\delta\right) + ... + tt'r'^{(2N-3)} \exp i\left(N-1\right)\delta \right], \tag{2.19}$$

and similarly, the total transmitted amplitude is given at point P' by:

$$E_t = E_0 tt' \left[1 + r'^2 \exp\left(i\delta\right) + r'^4 \exp\left(i2\delta\right) + ... + r'^{(2N-1)} \exp i\left(N-1\right)\delta \right]. \tag{2.20}$$

If we define

$$\delta = \frac{2\pi}{\lambda_0} 2n_f d \cos\theta_t, \tag{2.21}$$

we can write the Irradiance ratios of the Reflected and Transmitted beams:

$$\frac{I_r}{I_i} = \frac{F \sin^2\left(\frac{\delta}{2}\right)}{1 + F \sin^2\left(\frac{\delta}{2}\right)} \tag{2.22}$$

and

$$\frac{I_t}{I_i} = \frac{1}{1 + F \sin^2\left(\frac{\delta}{2}\right)}. \tag{2.23}$$

F is called the *coefficent of finesse*, and is defined as

$$F \equiv \frac{4R}{\left(1-R\right)^2}. \tag{2.24}$$

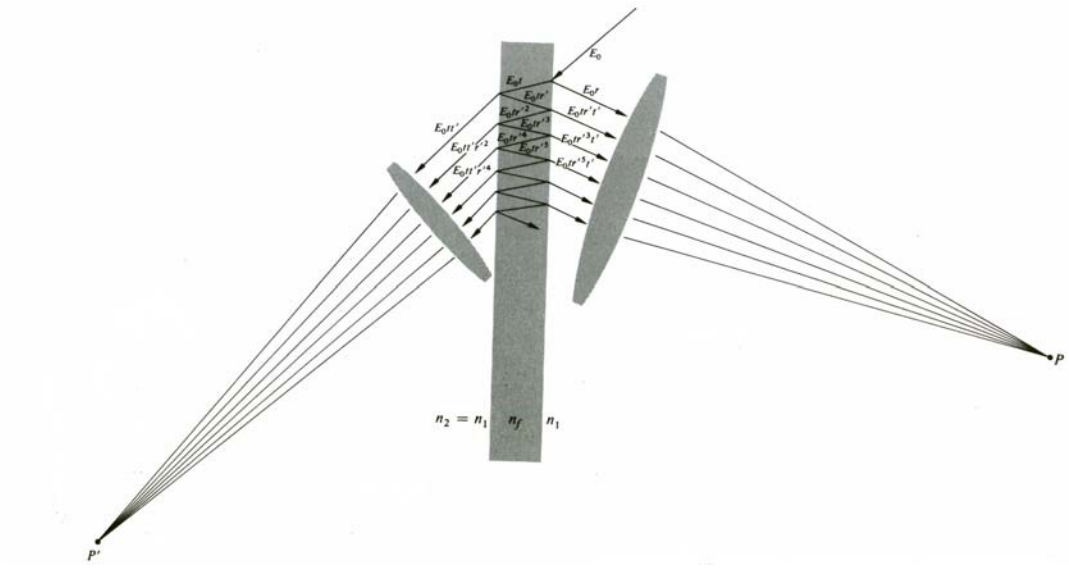

FIGURE 2.1. Multiple-beam interference from a parallel dielectric film.

2.1.3 Conservation of Energy

A fundamental law of physics that is well-preserved in Optics, Electromagnetics and Radiometry is asserted by James M. Palmer [7]: "*Everybody has to be someplace!*". Let A be the linear absorptance of a medium at a certain wavelength, and T and R its respective Transmittance and Reflectance. For normal incidence, we generally define:

$$R = \frac{I_r}{I_i} \tag{2.25}$$

and

$$T = \frac{I_t}{I_i}, \tag{2.26}$$

where I_0 is the Irradiance normally incident onto an interface, I_R is the normally reflected Irradiance from such interface, and I_T the Irradiance normally transmitted through said interface. Conservation of energy then states:

$$1 = A + R + T. \tag{2.27}$$

2.1.4 Complex Refractive Index

As a general rule, the refractive index of a medium is defined by the ratio of the speed of light in vacuum, to the speed of light in the medium. Thus:

$$N \equiv \frac{c}{v} = n - i\kappa. \tag{2.28}$$

N is called the *complex refractive index* of a medium. n is known as the *real part* or simply the *refractive index of the medium*, and κ is the *imaginary part* or *extinction coefficient* of a medium. For lossless dielectric media such as air, vacuum, glasses or our coating materials, $\kappa = 0$, resulting in a real refractive index, or $N = n \in \mathbb{R}$.

2.2 Optical Admittance and its Importance in Coating Design

2.2.1 Time-Harmonic Fields

Time-harmonic fields are waveforms periodic in time. If we are to think of smooth functions, without singularities, then time-harmonic waveforms are sinusoidal (or cosinusoidal) in nature. Electromagnetic waves are three-dimensional, and their direction of propagation is given by the unit vector $\widehat{s}$:

$$\widehat{s} = \alpha\widehat{x} + \beta\widehat{y} + \gamma\widehat{z}, \tag{2.29}$$

where α, β and γ are direction cosines for the wave [8]. The electric field propagating through dielectric media is then given by:

$$\overrightarrow{E} = \overrightarrow{E}_0 \exp\left[i\omega t - \left(\frac{2\pi N}{\lambda_0}\right)(\alpha x + \beta y + \gamma z)\right]. \tag{2.30}$$

However, for simplicity of argument, and to be consistent with the literature used at the University of Arizona [**?**] [**?**] [**?**], we assume for all interface inputs a harmonic plane wave of infinite extent, propagating parallel to $\widehat{z}$. We can then write both the electric and magnetic fields in a simpler form:

$$\overrightarrow{E} = \overrightarrow{E}_0 \exp\left[i\left(\omega t - kz\right)\right] \tag{2.31}$$

and

$$\overrightarrow{H} = \overrightarrow{H}_0 \exp\left[i\left(\omega t - kz\right)\right] \tag{2.32}$$

, where the wavenumber $k = \frac{2\pi N}{\lambda_0}$, real for dielectric media. Similarly, the angular frequency is related to the linear frequency f by $\omega = \frac{2\pi}{f}$. This notation is very convenient, because it allows us to incorporate any additional phase factors to our wave into the complex amplitudes in 2.31 and 2.32, as such:

$$\overrightarrow{E}_0 = \left|\overrightarrow{E}_0\right| \exp\left(i\phi\right) \tag{2.33}$$

and

$$\overrightarrow{H}_0 = \left|\overrightarrow{H}_0\right| \exp\left(i\phi\right) \tag{2.34}$$

2.2.2 Optical Admittance

For harmonic waves, $\overrightarrow{E}$, $\overrightarrow{H}$ and $\widehat{s}$ form a right-handed vector triad, which can be displayed (in S.I. units):

$$\frac{N}{c\mu}\left(\widehat{s}\times\overrightarrow{E}\right)=\overrightarrow{H}. \tag{2.35}$$

The quantity $\frac{N}{c\mu}$ has units of inverse impedance, or *admittance*. Indeed, this **is** the characteristic optical admittance of the medium:

$$\mathbf{y}\equiv\frac{N}{c\mu}=\sqrt{\left(\frac{\epsilon_0}{\mu_0}\right)} \tag{2.36}$$

and in free space or vacuum, this is given by [10]:

$$\mathbf{Y}_0=\frac{1}{377}\,\mathrm{S}=2.6544\times10^{-3}\,\mathrm{S}. \tag{2.37}$$

A simpler format is given by [11] Macleod, and states that for plane harmonic waves, we can write optical admittance as a ratio of scalars only:

$$\mathbf{y}=\frac{H}{E}=\frac{H_0}{E_0} \tag{2.38}$$

At optical frequencies ($\sim 10^{14}\,\mathrm{Hz}$), looking at Equation 2.9, we verify that $\mu_r=1$. As a consequence we can write [10]:

$$\mathbf{y}=N\mathbf{Y}_0 \tag{2.39}$$

and our vector triad becomes:

$$\overrightarrow{H}=\mathbf{y}\left(\widehat{s}\times\overrightarrow{E}\right)=N\mathbf{Y}_0\left(\widehat{s}\times\overrightarrow{E}\right).$$

Although optical admittance and refractive index are two distinct quantities, the change in units from characteristic admittance to free space is quite handy, for it allows us to utilize the **same number** for N and $\mathbf{y}$. This is a trick valid only at the high optical frequencies, useless in other realms, such as microwave frequencies [11].

2.2.3 Irradiance: The Time-Average Poynting Vector

Irradiance of an electromagnetic wave is defined by the instantaneous amount of power flow per unit area through an arbitrary cross-section of the material. Both direction and strength of energy flow are given by the Poynting vector:

$$\overrightarrow{S}=\overrightarrow{E}\times\overrightarrow{H}. \tag{2.40}$$

A few remarks must be made about the Poynting vector: it is not unique! This can be easily verified by choosing any arbitrary vector $\overrightarrow{A}$. Let $\overrightarrow{S'}$ be defined as $\overrightarrow{S'} = \overrightarrow{S} + \nabla \times \overrightarrow{A}$. Then $\nabla \cdot \overrightarrow{S} = \nabla \cdot \overrightarrow{S'} + \nabla \cdot \left(\nabla \times \overrightarrow{A} \right)$ and the result is $\nabla \cdot \overrightarrow{S} = \nabla \cdot \overrightarrow{S'}$. The total energy density of such electromagnetic field is:

$$u = \frac{1}{2} \left(\overrightarrow{E} \cdot \overrightarrow{D} + \overrightarrow{B} \cdot \overrightarrow{H} \right). \tag{2.41}$$

This is an important definition, because Poynting's theorem is a re-statement of conservation of energy:

$$\frac{\partial u}{\partial t} + \nabla \cdot \overrightarrow{S} + \overrightarrow{j} \cdot \overrightarrow{E} = 0. \tag{2.42}$$

For a harmonic plane wave, however, we can write irradiance on a scalar form [6]:

$$I = \frac{1}{2} \operatorname{Re} \left(\overrightarrow{E} \times \overrightarrow{H}^{*} \right) = \frac{1}{2} \operatorname{Re} \left(E_0 H_0^{*} \right). \tag{2.43}$$

Now, we can express irradiance in terms of the electric field strength and the optical admittance:

$$I = \frac{1}{2} \operatorname{Re} (\mathbf{y}) \left(E E^{*} \right) = \frac{1}{2} n \mathbf{Y}_0 E_0 E_0^{*}. \tag{2.44}$$

For the sake of completion, we also know that metallic coatings can be deposited as thin films. Metals are lossy by nature, and there are non-metallic coating materials which absorb electromagnetic energy as well [11]. Such energy losses are described by Beer's law

$$\frac{dI}{dz} = -\alpha I. \tag{2.45}$$

Notice that we are not using the well-known integrated form of Beer's law here, for it has the fallacy of only being valid in cases when α is very small. For stronger interactions between the optical field and the propagating medium, $\alpha = \alpha(I)$ and the average power absorbed is

$$\overline{P}_{abs} = \alpha(I) I, \tag{2.46}$$

which is then a nonlinear function of the incident irradiance itself inside the material at any point. Finally, the absorption coefficient is related to the imaginary part of the complex refractive index as follows:

$$\alpha(I) = \frac{4\pi\kappa(I)}{\lambda_0}. \tag{2.47a}$$

2.3 Refraction at a Simple Dielectric Boundary

Let us consider a an interface between two dielectric media of refractive indices n_0 and n_1, respectively. Let an harmonic electromagnetic plane wave be normally incident on this interface, propagating along the $\widehat{z}$ direction. The electric vector will be then parallel to the $\widehat{x}$ direction and the magnetic vector will be aligned with the $\widehat{y}$ direction for the transmitted and incident wavefronts ($-\widehat{y}$ for the reflected wavefront). The incident, transmitted and reflected time-harmonic scalar waveforms are then:

$$E_{incident} = E_i \exp\left[i\left(\omega t - \frac{2\pi n_0 z}{\lambda_0}\right)\right] \tag{2.48}$$

$$E_{transmitted} = E_t \exp\left[i\left(\omega t - \frac{2\pi n_1 z}{\lambda_0}\right)\right] \tag{2.49}$$

and

$$E_{reflected} = E_r \exp\left[i\left(\omega t + \frac{2\pi n_0 z}{\lambda_0}\right)\right] \tag{2.50}$$

The boundary conditions are then given by Born & Wolf [5], simplified by Macleod [10]. In essence, the tangential components of both the electric and magnetic vectors are continuous across the interface portrayed below:

$$E_i = E_t - E_r \tag{2.51}$$

and

$$H_i = H_t + H_r, \tag{2.52}$$

i.e., both the electric and magnetic vectors are continuous across the boundary 2.2. This is illustrated by Macleod below [11].Then

$$\mathbf{y}_0 \left(E_i - E_r\right) = \mathbf{y}_1 E_t$$

using Equation 2.51 we can then eliminate variables as needed and define amplitude reflection and transmission coefficients [10]:

$$\frac{E_r}{E_i} = \frac{\mathbf{y}_0 - \mathbf{y}_1}{\mathbf{y}_0 + \mathbf{y}_1} \equiv \rho \tag{2.53}$$

and

$$\frac{E_t}{E_i} = \frac{2\mathbf{y}_0}{\mathbf{y}_0 + \mathbf{y}_1} \equiv \tau. \tag{2.54}$$

Because of conservation of energy across the boundary itself, which is thin, the Poynting vector will be also continuous across the boundary. Then the total Irradiance I_{net} across the boundary will be:

$$I_{net} = \mathrm{Re}\left[\frac{1}{2} E_i \left(\mathbf{y}_1 E_t\right)^*\right] = \frac{1}{2}\mathbf{y}_0 E_i E_i^* \left(1 - \rho^2\right) = \frac{1}{2}\mathbf{y}_0 E_i E_i^* \left(\frac{\mathbf{y}_1}{\mathbf{y}_0}\right)\tau^2 \tag{2.55}$$

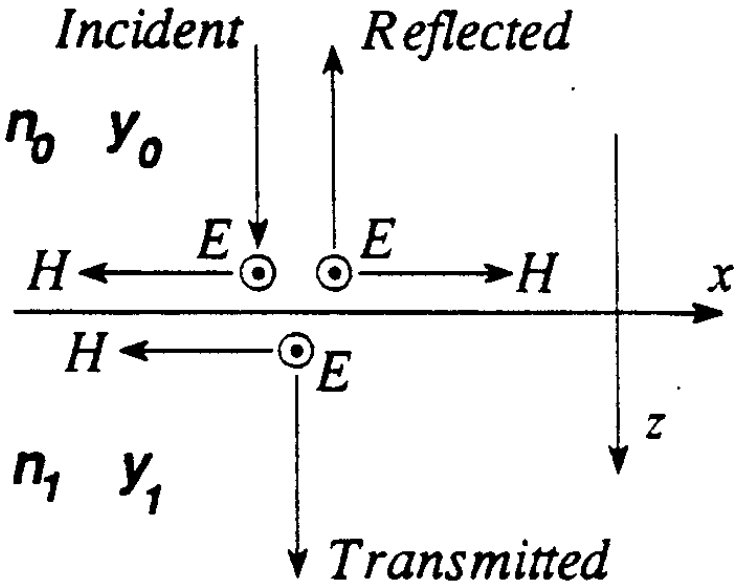

FIGURE 2.2. Convention for positive field directions for waves at an interface.

and the quantities reflectance R and transmittance T from equations 2.25 and 2.26 can now be revisited:

$$R = \frac{I_r}{I_i} = \rho^2 = \left(\frac{\mathbf{y}_0 - \mathbf{y}_1}{\mathbf{y}_0 + \mathbf{y}_1}\right)^2 \tag{2.56}$$

and

$$T = \frac{I_t}{I_i} = \frac{\mathbf{y}_1}{\mathbf{y}_0}\tau^2 = \frac{4\mathbf{y}_0\mathbf{y}_1}{(\mathbf{y}_0 + \mathbf{y}_1)^2}. \tag{2.57}$$

Of course, if the material is an absorber, $\mathbf{y}_1$ is then replaced by the admittance $n_1 - i\kappa$ and the reflectance becomes:

$$R_{absorber} = \left[\frac{(n_0 - n_1)^2 + \kappa^2}{(n_0 + n_1)^2 + \kappa^2}\right] \tag{2.58}$$

and of course, the conservation of energy statement

$$1 = A + R + T. \tag{2.59}$$

is still valid.

2.4 Reflectance of a Thin Film

Although we are accustomed to referring to optical materials via their bulk properties, we must now start differentiating the bulk material from the thin film. A film or coating is said to be optically **thin** whenever interference effects can be detected in the electromagnetic waves it transmits or reflects; it is said to be **thick** when such effects are not detectable [11]. As a rule of thumb, we can expect substrates to be thick, or macroscopic, and coatings to be thin or microscopic, usually at a fraction of a wavelength of light in question.

Now, when speaking about bulk materials, the surface admittance and the admittance within the material are one and the same. For the thin film, however, that is not so, because the total electric and magnetic fields are modified by multiple partially-reflected or partially-transmitted waves interfering with one another. Indeed, the admittance of a thin film will depend on a combination of factors including the layer thicknesses and admittance of the bulk substrate on which it is deposited. On a multilayer stack, it is common to find a surface admittance completely different from the bulk admittances of any of the materials used by themselves. Indeed, by now the reader must have realized that the thin film acts as an **admittance transformer**. Its surface admittance can singularly characterize the optical response of the coating in question.

Surface admittances are calculated in simulation (the Essential Macleod® Software included) via characteristic matrices which relate the electromagnetic fields in both sides of the thin film coating, and we present that theory on the following section, from H. Angus Macleod's text [10].

2.4.1 Characteristic Matrices

The reflectance of a multi-layer stack is calculated by replacing the multiple layers by a single equivalent admittance $\mathbf{Y}$, defined to be the ratio of the total tangential magnetic and electric fields. Of course, this works better if we normalize the output electric field to unity and the output magnetic field to $\mathbf{y}_{sub}$. Keeping 2.38 in mind then leads us to:

$$\mathbf{Y} = \frac{H}{E} = \frac{C}{B} \tag{2.60}$$

and:

$$\begin{bmatrix} B \\ C \end{bmatrix} = \left\{ \prod_{j=1}^{q} \begin{bmatrix} \cos\delta_j & \frac{i\sin\delta_j}{\mathbf{y}_j} \\ i\mathbf{y}_j \sin\delta_j & \cos\delta_j \end{bmatrix} \right\} \begin{bmatrix} 1 \\ \mathbf{y}_{sub} \end{bmatrix}, \tag{2.61}$$

where the phase thickness of the wave δ_j is given by:

$$\delta_j = \frac{2\pi \mathbf{y}_j d_j}{\lambda_0}, \tag{2.62}$$

d_j is the j-th layer geometrical thickness, and $\mathbf{y}_j = (n_j - i\kappa_j)$. If the j-th layer is next to the substrate, the order of multiplication must be:

$$\begin{bmatrix} B \\ C \end{bmatrix} = [M_1]\,[M_2]\,...\,[M_j] \begin{bmatrix} 1 \\ \mathbf{y}_{sub} \end{bmatrix}. \tag{2.63}$$

Now all important parameters can be derived, i.e. Reflectance:

$$R = \left(\frac{\mathbf{y}_0 B - C}{\mathbf{y}_0 B + C}\right)\left(\frac{\mathbf{y}_0 B - C}{\mathbf{y}_0 B + C}\right)^*; \tag{2.64}$$

Transmittance:

$$T = \frac{4\mathbf{y}_0 \,\mathrm{Re}\,(\mathbf{y}_{sub})}{(\mathbf{y}_0 B + C)\,(\mathbf{y}_0 B + C)^*}; \tag{2.65}$$

and Absorptance:

$$A = \frac{4\mathbf{y}_0 \,\mathrm{Re}\,(BC^* - \mathbf{y}_{sub})}{(\mathbf{y}_0 B + C)\,(\mathbf{y}_0 B + C)^*}. \tag{2.66}$$

Potential Transmittance of a thin film coating is defined as the ratio of the irradiance leaving the coating to the net irradiance 2.55 entering the stack, and it is a useful figure of merit to assess losses in multilayer coatings:

$$\psi = \frac{I_{exit}}{I_{net}} = \frac{T}{(1-R)} = \frac{\mathrm{Re}\,(\mathbf{y}_{sub})}{\mathrm{Re}\,(BC^*)}. \tag{2.67}$$

Finally, the phase shifts on reflection:

$$\varphi = \arctan\left(\frac{\mathrm{Im}\,[\mathbf{y}_{sub}\,(BC^* - CB^*)]}{(\mathbf{y}_{sub}^2 BB^* - CC^*)}\right) \tag{2.68}$$

and transmission:

$$\phi = \arctan\left[\frac{-\,\mathrm{Im}\,(\mathbf{y}_0 B + C)}{\mathrm{Re}\,(\mathbf{y}_0 B + C)}\right]. \tag{2.69}$$

2.4.2 The Quarterwave Rule and AR-Coating Design

To understand the quarterwave rule we must understand the concept of constructive and destructive interference.

Chapter 3

COATING DEPOSITION PROCESSES

3.1 Physical Vapor Deposition

[sggsggfsg]

3.2 Spin Coating

[ssdsad]

3.3 Dip Coating

[dsdasdsd]

Chapter 4

ANTI-REFLECTION COATING DESIGNS FOR MAESTRO

The following are prescription designs and characteristic curves for different anti-reflection filters developed for the M.A.E.S.T.R.O. spectrograph. We have used the Essential Macleod Software for Windows, version 6.3F. The software is very fast and flexible, and allows for custom material additions to its database.

4.1 The Stilburn Design

The inspiration for most of the designs presented here was a coating designed by James Stilburn of the Herzberg Institute of Astrophysics and the National Research Council of Canada [9]. This was the first AR-coating in astronomy to make use of a combination of Sol-Gel and a hard coating material. The design wavelength was 670 nm and the prescription was a quarterwave stack as follows:

$$AIR|SILICA\_SOLGEL|MgF_2|FUSED\_SILICA. \tag{4.1}$$

The performance plot of this coating is shown on Figure 4.1. Although Dr. Stilburn's design is a milestone of simplicity and performance, there are still unaddressed issues by this filter. One problem with this coating is that for wavelengths shorter than 450 nm, the coating's performance decreases quite rapidly, which can make utilization in the deep blue and near UV impractical. It also contains a layer of solgel exposed to the environment, which makes it frail, susceptible to humidity-induced degradation, and difficult to clean even under ideal laboratory conditions. Last but not least, this coating is optimal only for Fused Silica substrates. Such unresolved issues, coupled with the needs of the MAESTRO instrument were the driving force behind my research.

4.2 The Choice of a Moisture Barrier

The choice of a moisture barrier was key to all posterior considerations, since the solgel layer must be protected from humidity and atmospheric impurities. The perfect moisture barrier would be transparent to our electromagnetic spectrum of interest, completely impermeable to humidity and as easy to clean as uncoated glass. Several choices of compounds must be considered here. Silica solgel is very useful to create

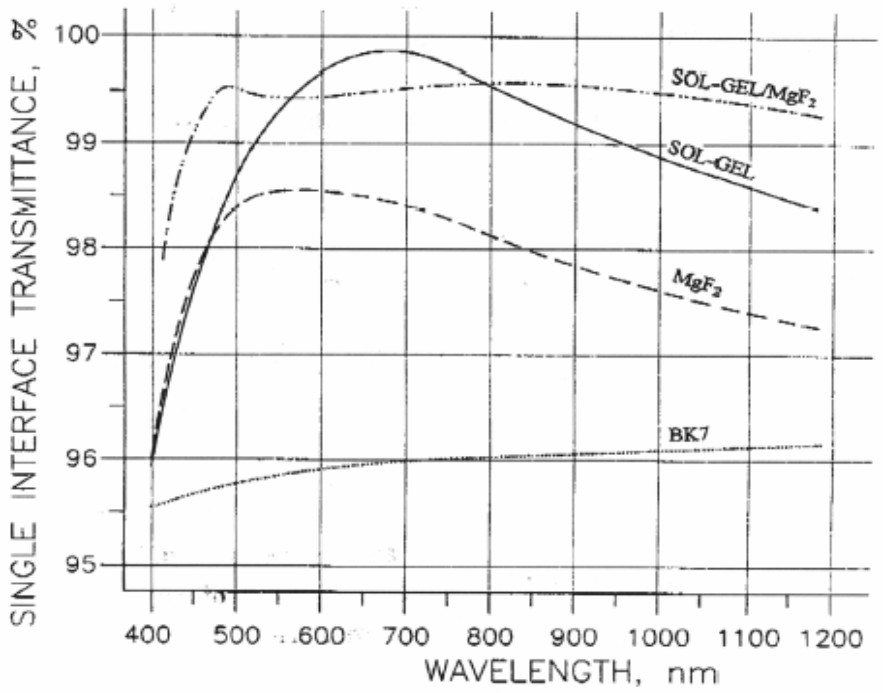

FIGURE 4.1. Comparison plot between traditional AR coatings and Stilburn design.

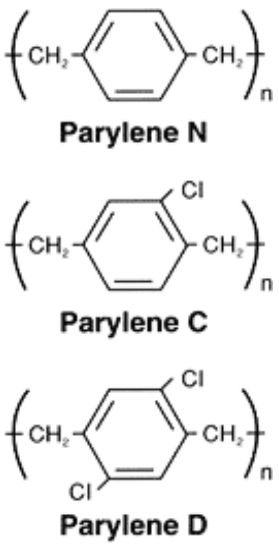

FIGURE 4.2. Parylene structures.

AR-stacks on glassy substrates due to its $n_D = 1.22$ refractive index, as seen above in Figure 4.1. However, silica solgel layers are porous, and therefore frail. Such layers have a very short lifetime against hygrometrical environmental changes and are virtually impossible to clean, even from ordinary atmospherically-carried dust.

The group of substances we considered were well-known optically-transmissive polymers. Polycarbonates are particularly tempting due to their ease of deposition, low cost, and virtually zero maintenance needed for decades. We abandoned this polycarbonates, because of their opacicity at wavelengths shorter than 380 nm, which made them an impractical choice to fulfill MAESTRO's requirements.

Parylene-C solutions were also considered since they have been used for years as moisture and chemical barriers in semiconductor circuits and biomedical devices. Parylenes are a generic name for a a series of polymers, based on the basic form, poly-paraxylylene, also known as Parylene-N. The basic chemical structure of this group is illustrated on Figure 4.2 Parylene-C possesses a nominal Moisture Vapor Transmission of $1.693\,5 \times 10^{-4} \frac{\mathrm{n\,g}}{\mathrm{Pa\,s\,m}}$ at 90% Relative Humidity, 37 °C. But although stable indoors, Parylenes are not recommended for long term use outdoors, for they tend to degrade when exposed to UV sunlight [13].

Another alternative has been suggested by Stilburn himself, and it consists of treating the sol-gel coating with a solution of dichlorodimethylsilane (DDMS) in ethanol, at a concentration of $5ppm$ [14]. The same solution must also be used for cleaning, but extensive research on the topic is still being carried out. However, organo-silanes, particularly in their organo-halide-silane form seemed to be promising compounds for our purpose.

An epiphany presented itself while I watched a History Channel© segment about George Washington and his famous frown, about a year ago. It was mentioned that General Washington suffered from bad teeth decay, not unlike most people in the late 18th century. There was little or no technology involving modern medicine or dentistry at the time, so extraction was often the only treatment available before cavities evolved into abcesses, which in turn could easily kill the patient in those days. Since chemistry and the science of synthetic materials was non-existing, dentures were poorly fitted, uncomfortable, crude contraptions made of wood and wire, available only to the wealthy. Of course, it helps to have dentists in the family, and so I spoke with my youngest brother, whom confirmed to me that dentures today are made of ceramics.

The relationship with dentistry is quite significant. Dentures must last years under mechanical wear and under the most adverse conditions. Moisture must be repelled to avoid degradation of the denture substrate. The low pH environment of the human mouth is second only to the stomach, and dentures still must be able to chew through a steak, resist ice water, hot coffee and ice cream during the same meal. An environmental barrier of this quality, if transparent to our spectral needs, would be ideal to any coating developed. We then looked for the leading investigator of moisture and chemical barriers in dental ceramics in the United States, which turned out to be Professor Prabhat K. Gupta of Ohio State University. Dr. Gupta has provided with a reprint of one of his recent papers, and a material under active investigation by his group is triethoxy(perfluoroalkylethyl) silane, another organo-halide-silane compound [15].

Our search was short but productive, thanks to Prof. Bechtold, who introduced us to the product line of Gelest, Inc. From their catalog, we have chosen the Aquaphobe® CF. "Aquaphobe® CF is a chlorine-terminated, polyfluoroalkylmethylsiloxane oligomer" [16]. Prepared in a 2.0% solution in ethanol by molecular weight, it presents a refractive index $n_D \approx 1.35$, which can be easily incorporated onto our coating designs. Our first tests involved drop-coating $1\,\text{in}^2$ samples of flat borosilicate glass with Aquaphobe® CF solution. We then measured the spectral refractive index of the Aquaphobe® CF layer using a Cary 500 Spectrophotometer. The resulting plot of refractive index versus wavelength is shown below on Figure 4.3. Although we only gathered precision data for a few wavelengths, the Essential Macleod software can work with limited support functions, by interpolating or extrapolating them as needed, via cubic splines.

4.3 The Coyote® Design

We modified Stilburn's original design as to broaden the coating characteristics for shorter wavelengths. The Coyote® prescription is based on the standard (Air|HLH|Glass) form for anti-reflection coatings. It was design to be an optimal, low-cost AR-coating

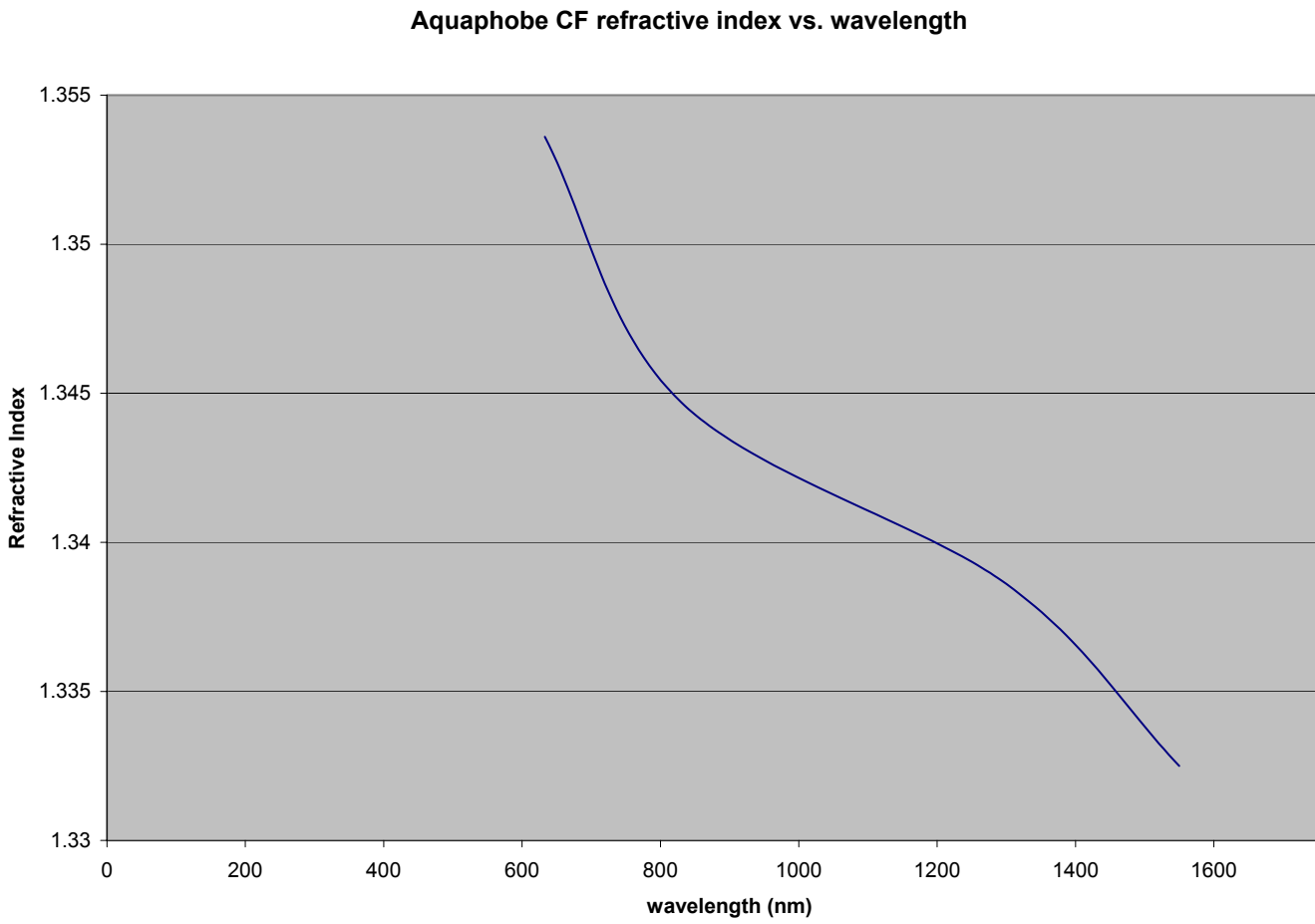

FIGURE 4.3. Refractive index vs. wavelength of Aquaphobe CF 2% solution.

Design: FUS_SIL5
Reference Wavelength: 510.00
Incident Angle: 0.0

Layer	Material	Refractive Index	Extinction Coefficient	Optical Thickness
Medium	Air	1.0000	0.0000000	
1	GELEST AQUAPHOBE	1.3536	0.0000000	0.00144713
2	SOL-GEL 50%	1.2311	0.0000000	0.24306140
3	MgF2	1.3845	0.0000000	0.22075280
Substrate	Fused Silica	1.4622	0.0000000	

FIGURE 4.4. Prescription of Coyote® AR-coating design.

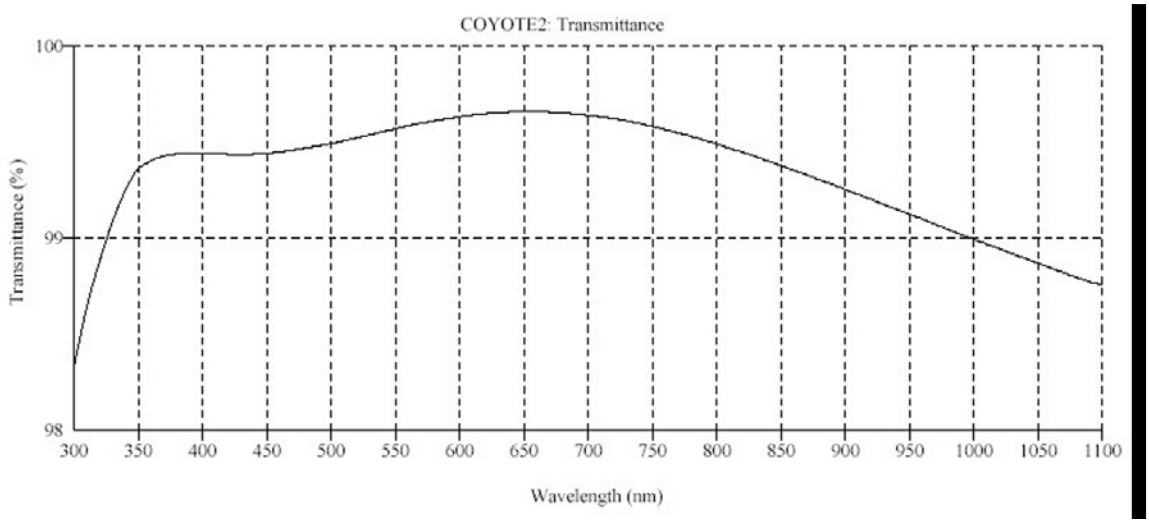

FIGURE 4.5. Performance plot for Coyote® AR-coating design.

useful throughout the entire spectral band visible from the Earth's surface, on a fused silica substrate. The addition of the Silane-based Gelest Aquaphobe compound added greater resistance to humidity and made cleaning easier. An optimization was forced via Simulated Annealing, using the Essential Macleod software, with a shorter center wavelength of 510 nm. The prescription is shown on Figure 4.4 and performance plot depicted on Figure 4.5.

4.4 The Scorpio® Design

Scorpio® was optimized for glass substrates of higher refractive index, about 1.6, made by the OHARA company. Coating characteristics were broadened by the addition of LaF3 as an extra material. The generating quarterwave stack is still centered at 510 nm. Optimization had the following starting point, executed by the

Design: DBACK3
Reference Wavelength: 510.00
Incident Angle: 0.0

Layer	Material	Refractive Index	Extinction Coefficient	Optical Thickness
Medium	Air	1.0000	0.0000000	
1	GELEST_AQUAPHOBE	1.3536	0.0000000	0.00189886
2	SOL-GEL 50%	1.2311	0.0000000	0.22775420
3	MqF2	1.3845	0.0000000	0.23588290
4	LaF3	1.5760	0.0000000	0.74998300
Substrate	OHARA PBM18Y Glass	1.6035	0.0000000	

FIGURE 4.6. Prescription for the Scorpio® AR-coating.

OPTIMAC™ algorithm:

$$AIR|Sol\_Gel|MgF_2|LaF_3|OHARA\_PBM18Y\_GLASS.$$

The final prescription and performance plot are shown below in Figures 4.6 and 4.7. This design was modified with the addition of an extra half-wave layer of Silane-organic between the last Sol-Gel and air, as a hydrophobic, protective layer.

4.5 The Gila® Design

The Gila® coating design is optimized for Calcium Fluoride substrates, since those behave quite differently from Fused Silica substrates, despite their similar refractive index for d-light. The Aquaphobe® compound is again used as a protective layer to the Sol-Gel component. This coating was designed specifically for the calcium fluoride component of the injection optical subsystem, custom figured by Tucson Optical Research Corporation. Its prescription is depicted below on Figure 4.8 and performance on Figure 4.9.

4.6 The Tarantula® Design

Optimized for borosilicate glass substrates ($n = 1.52$), this design is also centered at the 510 nm wavelength. The staring point was also a quaterwave structure of the type:

$$Air|L|I|H|BK7\_Glass$$

The current prescription and performance plot are shown below on Figures 4.10 and 4.11. This design is still being modified with the addition of an extra half-wave layer of a Silane-organic compound between the last MgF2 and air, as a hydrophobic, protective layer.

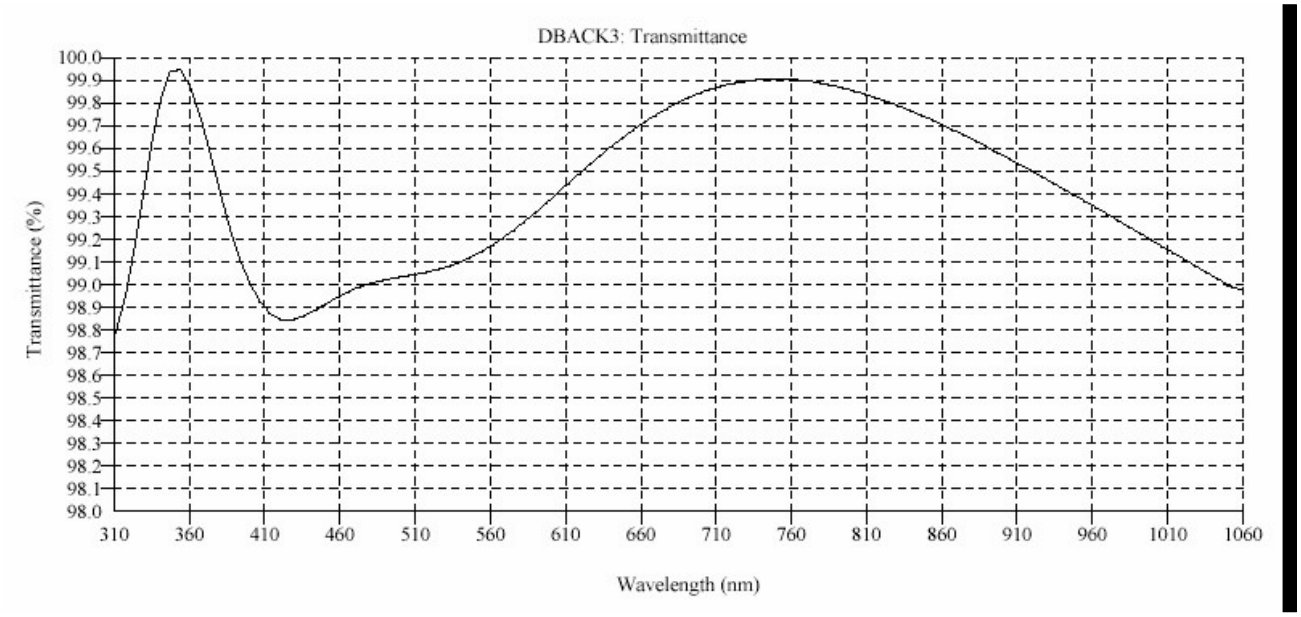

FIGURE 4.7. Performance plot for the Scorpio® AR-coating design.

Design: GILA9
Reference Wavelength: 510.00
Incident Angle: 0.0

Layer	Material	Refractive Index	Extinction Coefficient	Optical Thickness
Medium	Air	1.0000	0.0000000	
1	GELEST_AQUAPHOBE	1.3536	0.0000000	0.00081515
2	SOL-GEL 50%	1.2311	0.0000000	0.24640250
3	MgF2	1.3845	0.0000000	0.02143531
4	GELEST_AQUAPHOBE	1.3536	0.0000000	0.19679040
Substrate	CaF2P20	1.4366	0.0000000	

FIGURE 4.8. Prescription for the Gila® AR-coating design.

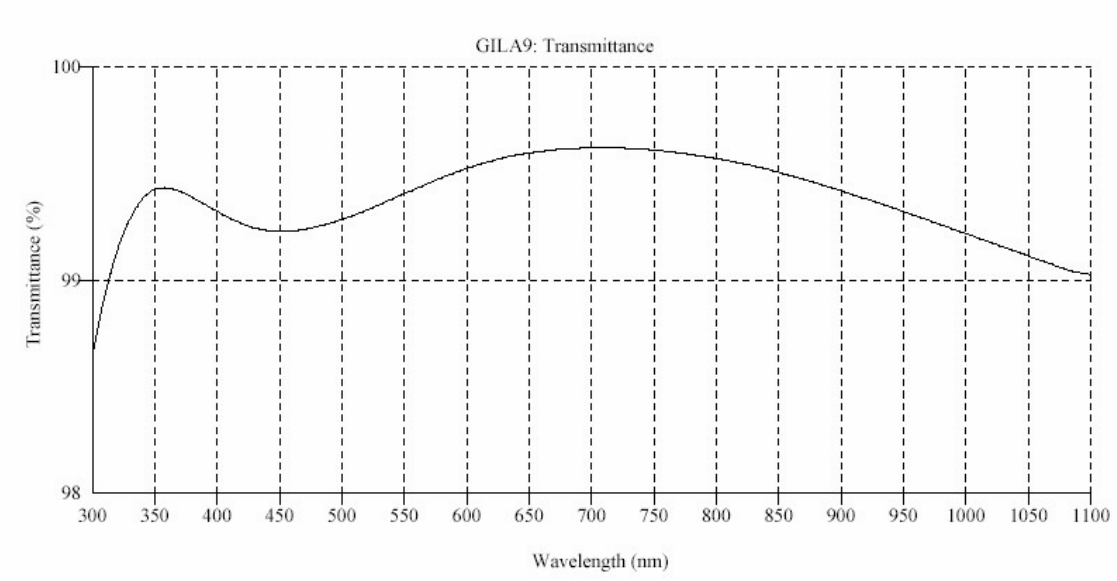

FIGURE 4.9. Performance of Gila® AR-coating design.

Design: BK7
Reference Wavelength: 510.00
Incident Angle: 0.0

Layer	Material	Refractive Index	Extinction Coefficient	Optical Thickness
Medium	Air	1.0000	0.0000000	
1	MgF2	1.3845	0.0000000	0.00039675
2	SOL-GEL 50%	1.2311	0.0000000	0.26232070
3	SiO2	1.4618	0.0000000	0.05037177
4	MgF2	1.3845	0.0000000	0.04310897
5	SOL-GEL 50%	1.2311	0.0000000	0.04919391
6	MgF2	1.3845	0.0000000	0.01103199
7	SiO2	1.4618	0.0000000	0.21018470
8	MgF2	1.3845	0.0000000	0.01282364
Substrate	Glass	1.5209	0.0000000	

FIGURE 4.10. Prescription for Tarantula® AR-coating design.

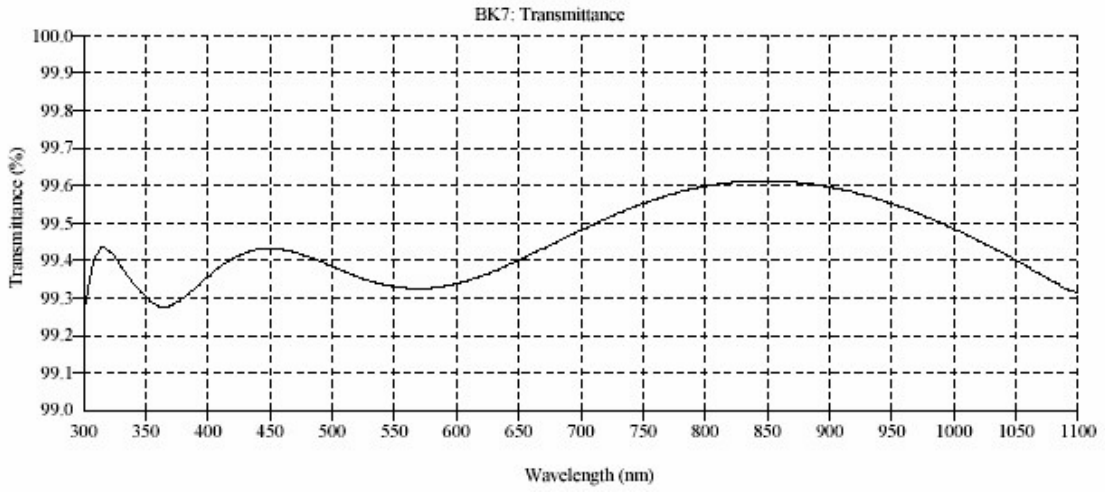

FIGURE 4.11. Performance plot for Tarantula® AR-coating design.

Chapter 5

MANUFACTURING OF THE COYOTE® AR-FILTER

5.1 Preliminary Environmental Tests

The purpose of this test was solely to determine whether the Silane-based Aquaphobe would hold against the second layer of silica sol-gel, as well as prevent degradation from unfriendly environmental conditions. Due to materiel, cost and time limitations, we have made some modifications on the original COYOTE® prescription listed above. The substrates used were $1\,\text{in}^2$ microscope slides, made of borosilicate BK7 glass. The first layer, made of Magnesium Fluoride, was precision-deposited via Physical Vapor Deposition. The second layer, made of a 50% solution of silica sol-gel, was drop-coated onto the first layer. Once the second layer is cured, a day later [9], the Aquaphobe solution is drop-coated onto the second layer, and subsequently baked for 15 minutes in a vacuum oven. The shortcomings of this procedure are quite obvious: drop coating is not a precision deposition process, so the resulting thicknesses may not be appropriate for sensitive prescriptions.

The samples tested for spectral transmission over the wavelength range of interest, using a device. Four samples were selected for this purpose, S1 and S2 did not survive the first Sol-Gel deposition on top of the Magnesium Fluoride layer. The instrument used to test for spectral transmission was a Varian Cary 500 Spectrophotometer, pictured below on Figures 5.1 and 5.2 [17].

The two remaining deposited samples were then environmentally tested in four-step cycles:

1) Samples were cooled down to -20 °C for 12 hours, insulated from humidity or contamination.

2) Samples were warmed up to 35 °C for 12 hours, insulated from humidity or contamination.

3) Samples were cooled down to room temperature for 12 hours, exposed to humidity and contamination.

4) Samples were cooled down to 4 °C for 12 hours, in a fridge, leaking water.

Once this cycle was repeated 4 times, samples were re-tested for spectral transmission over the wavelength range of interest, using the same device above. A third measurement followed a posteriori made two weeks later, samples kept in isolation during the intermediate time. The spectral transmissions are plotted on the same graph 5.3 below for quick comparison and analysis.

Although this was just a preliminary experiment, with only a few samples, some conclusions can be derived from this plot:

FIGURE 5.1. The CARY500 Spectrophotometer

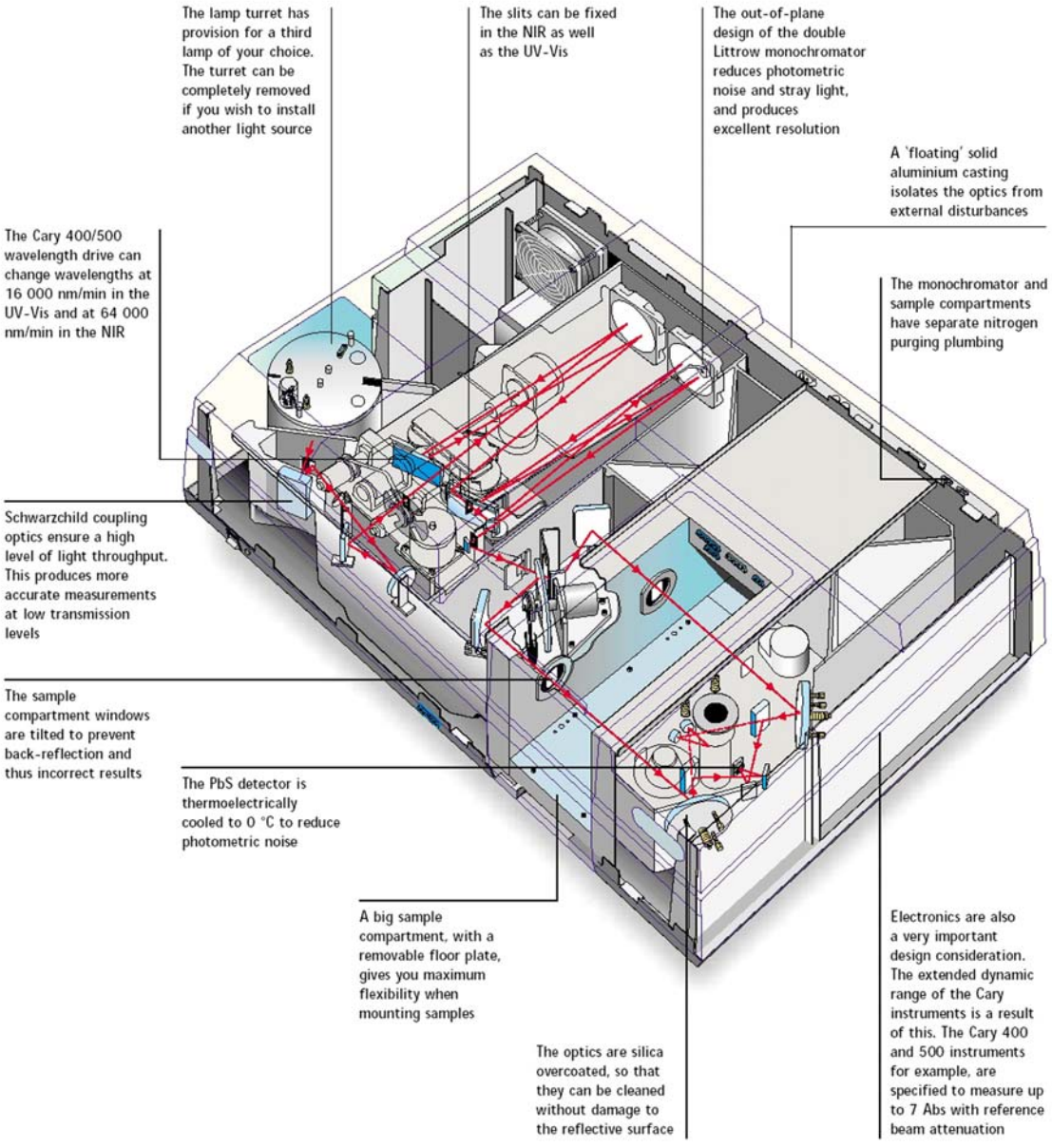

FIGURE 5.2. Schematic view of the Cary 500 Spectrophotometer

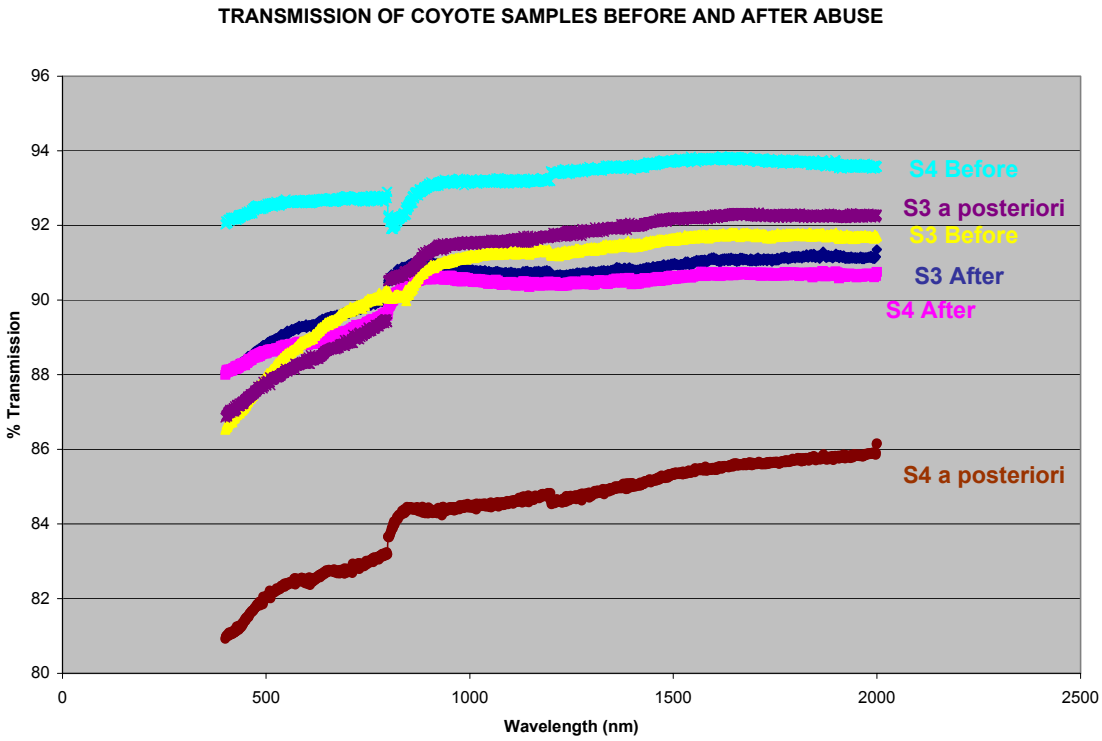

FIGURE 5.3. Transmission of COYOTE sample runs after environmental tests.

1) Curve shapes do not change after abuse sessions. This means that the coating is, in essence, unchanged in its nature by the abuse suffered.

2) Sample 4 suffered the greatest shift offset, about 4-5% between each measurement. Since our unit suffered multiple repairs and calibrations over the past 5 weeks, it is possible that a systematic error consistent with the intrinsic error of the instrument is to blame. This would also be consistent with most error expectancies for experimental spectrophotometry. Sample S3 seems to support that theory. However, we now know that Sample S4 may have suffered further degradation with time due to being touched with unprotected hands during the first mmeasurement, a fact confirmed by our operator. The primary defense of the human immune system is the low pH of the skin, which is laced with sweat and other oils, forming an acidic organic solution which acts as a biological barrier against infections. The time-continuous degradation of Sample 4 seems to support this theory, since it would take a finite time for human hand secretions to corrode through the coating layers.

3) The general curve shapes are not what we expected from the design shown on the first section of this document. Again, this preliminary drop-coating experiment was done with the intention of evaluating the adsorption between layers, as well as the environmental resiliency of the COYOTE® coating structure. We have then carefully deposited thickness-controlled layers of sol-gel and Aquaphobe on glass, via dip-coating procedure. Those were tested again on the Cary 500 spectrophotometer and modeled with the Essential Macleod software for validation. Results shall be added and discussed in section 5.3.

5.2 Dipping Calibration Procedure

For this procedure, we have utilized the dip coating hardware loaned to us by Prof. Dunbar Birnie, III. It consists of a motor and driver, manufactured by Oriental Motor, Inc., in the late 1980s. We have used motor 5RK40RGK-A2, serial number 25698. It is rated to a maximum output of 40 W at 1.5 A and 100 V. It can operate at either 50 or 60 Hz and rectified at a capacitance of 15 μF. The apparatus and our rigging are shown on Figures 5.4 and 5.5.The lab jack and book stack are low-tech solutions to raising the solution container to the needed height for dipping, above the lower limit switch of the encoder apparatus. The velocity of the motor going up or down is regulated by two different knobs, on the lower right of the controller box. Motor speeds are feedback-controlled by analog encoders connected to the servo mechanism. A small beaker with solution was placed on top of the lab jack platform, and the borosilicate glass samples are lowered onto the dipping solution. Glass samples were cut to be 0.5 in $\times$ 1 in in size, and prepared in a clean environment. Samples were then clean in an acetone bath for fifteen minutes and then run through the ultrasonic cleaner, untouched by bare hands throughout the entire process.

Samples were lowered onto the solution at the motor's maximum speed, namely

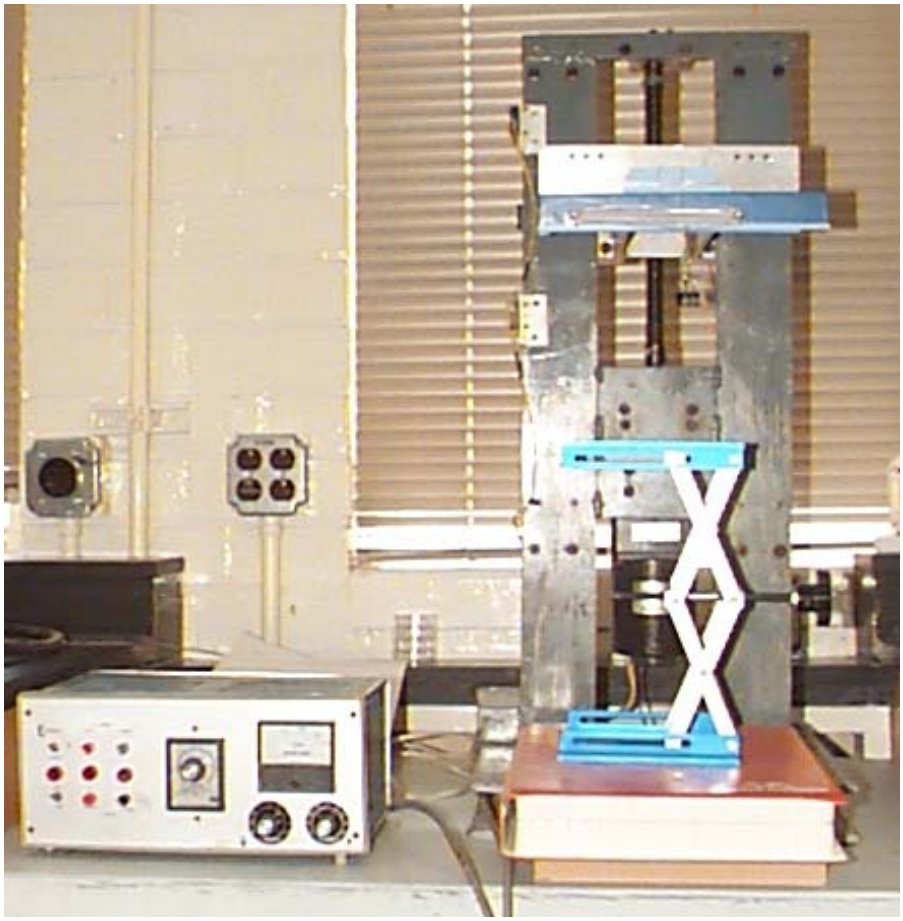

FIGURE 5.4. Dip-coating apparatus and analog driver to its left.

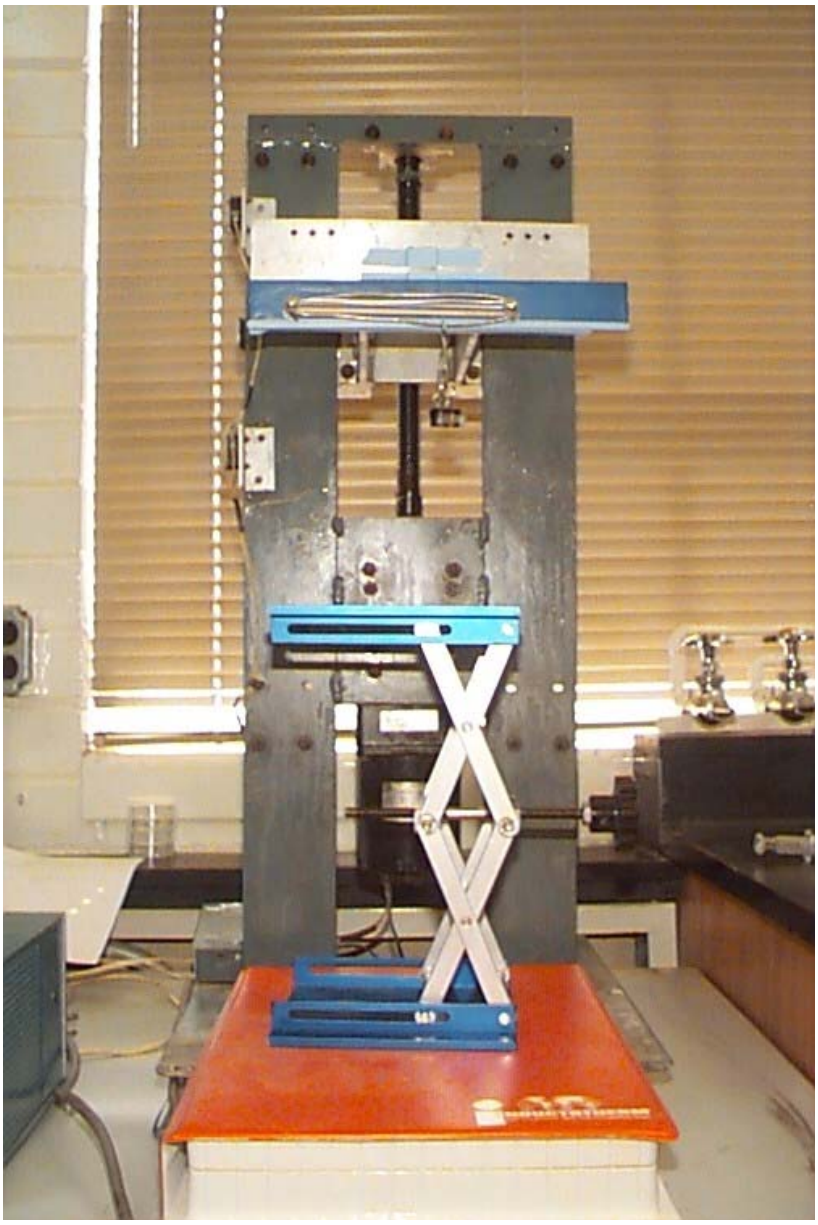

FIGURE 5.5. Closer look at dipping apparatus. Paperclip is sample holder.

FIGURE 5.6. KLA-Tencor Alpha-step 500 surface profiler.

1650 rpm. We have no real way of gauging the speed of the elevator platform; our only feedback is the number of revolutions per minute performed by the acme screw of the motor at any time, so our data must be calibrated to that reference. The resolution of the analog motor speed reader is 50 rpm. Twelve samples of each solution (solgel and Aquaphobe®) were dipped at 1650 rpm, and removed from the solution at speeds: 100, 150, 200, 300, 400, 500, 600, 700, 800, 900, 1000 and 1100 rpm. Sample film thicknesses were then tested using a KLA-Tencor Alpha-step 500 stylus surface profiler, depicted in Figure 5.6. The stylus has a resolution of 1 Å and a guaranteed 10 Å or 0.1% repeatability. Resulting thicknesses are plotted on Figure **??** below and are used in the following sections.

5.3 Second Environmmental Testing Cycle

Inspired by the data from the previous sections from this chapter, we repeated the evironmental test described on section 5.1, with a larger number of samples and a

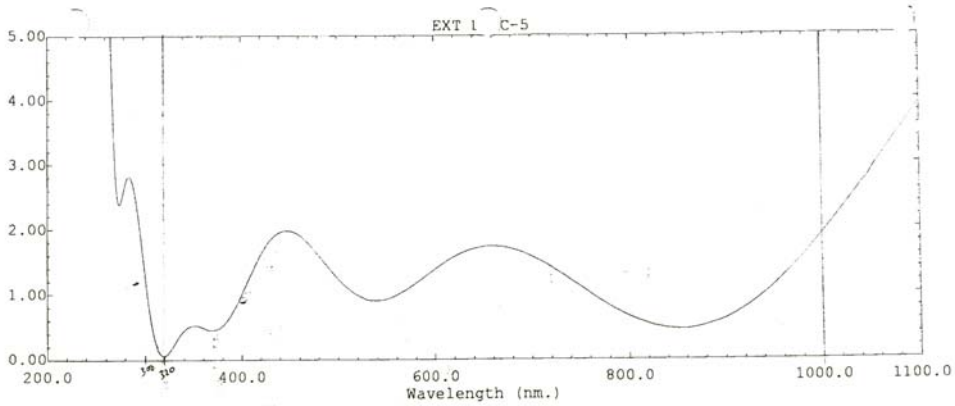

FIGURE 5.7. Characteristic Reflectance curve for ZC&R BBAR coating on fused silica substrate.

broader distribution of deposition and test conditions.

1) Samples were cooled down to -20 °C for 12 hours, insulated from humidity or contamination.

2) Samples were warmed up to 35 °C for 12 hours, insulated from humidity or contamination.

3) Samples were cooled down to room temperature for 12 hours, exposed to humidity and contamination.

4) Samples were cooled down to 4 °C for 12 hours, in a fridge, leaking water.

5.4 Coating Test Silica Lenses

sdjkfsfkdfksfdfhs

5.5 Comparisons with Commercially Available AR-Filters

The best commercial alternative to our custom line of astronomical coatings we have found to date is the broadband AR-coating provided by ZC&R Coatings for Optics, Inc., a company from Los Angeles, California [18]. This is the coating used on the custom optics of the 90-inch Prime Focus Instrument [19]. It is optimized for a fused silica substrate. Its reflectance characteristic curve is shown in Figure 5.7 below.

Compared to our 3-layer COYOTE design, however, this performance is not impressive. Since it is always better to compare apples with apples, a reflectance plot of COYOTE on fused silica is shown below on Figure 5.8:

This plot already defeats the "one coating for all substrates" idea. The performance of the BBAR ZC&R coating worsens when deposited on surfaces other than the ideal fused silica design substrate. However, at an estimated cost of US$ 15,000.00

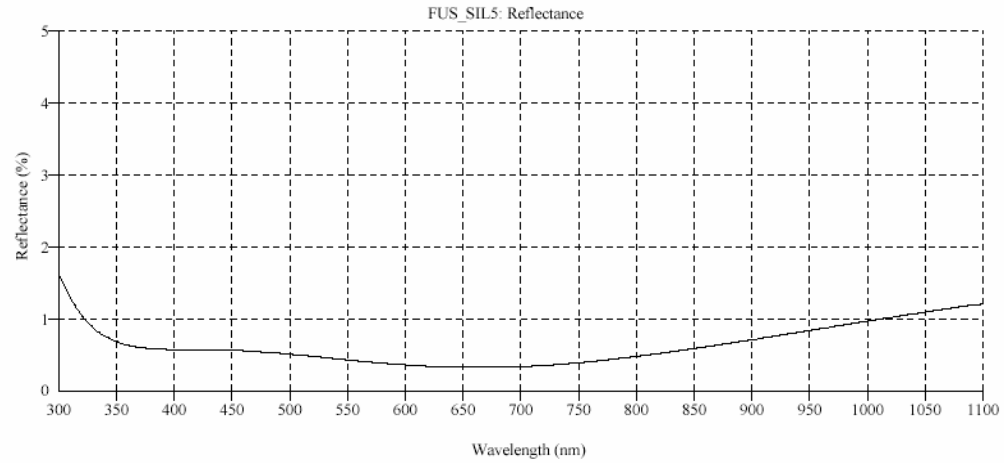

FIGURE 5.8. Reflectance plot for COYOTE coating on a fused silica substrate.

for our six large pieces, both surfaces included, this coating comes with a tempting price tag.

Another cost effective solution would be to approach the coating issue with simplicity and use a single layer of magnesium fluoride. At an estimated cost of $ 4,000.00 for the whole lot, this sounds like a bargain. However, as the plots of Figures 5.9 and 5.10 below show, cheap is not always a good idea, especially nearing the edge of our band of interest.

Since MgF2 is not hydrophobic and not particularly great outside the 400nm-700nm range, its performance is, of course, less than ideal for our needs. The greatest disadvantages of our custom coatings are two: 1) they cannot be deposited using a single process, by one single company; 2) Their cost. It would be ideal if either Optical Shop within the University of Arizona had optical coating deposition capability. Surprisingly, for an institution which claims to be a world leader in the area, research on coating depositions, novel materials and process optimizations has been virtually dead at the UA for at least a decade. The cost is quite high. Last Spring's estimates for a single layer of sol-gel alone, dip-coated, is about US$ 9,000.00 per layer per lot, plus tooling. Adding another dip-coated layer of Aquaphobe would approximately double the cost mentioned above. If we include LaF3 and MgF2 layers, runs could run at US$ 4,000.00 per layer. A conservative cost estimate would be about US$ 30,000.00 including shipping and tooling.

The benefits of our custom coating line are two-fold: their throughput performance is optimized for each substrate, with a minimum of layers used. The second is their environmental resistance to the degradation caused by the elements, most specifically degradation caused by humidity, especially on the natively hydrolitic sol-gel layers.

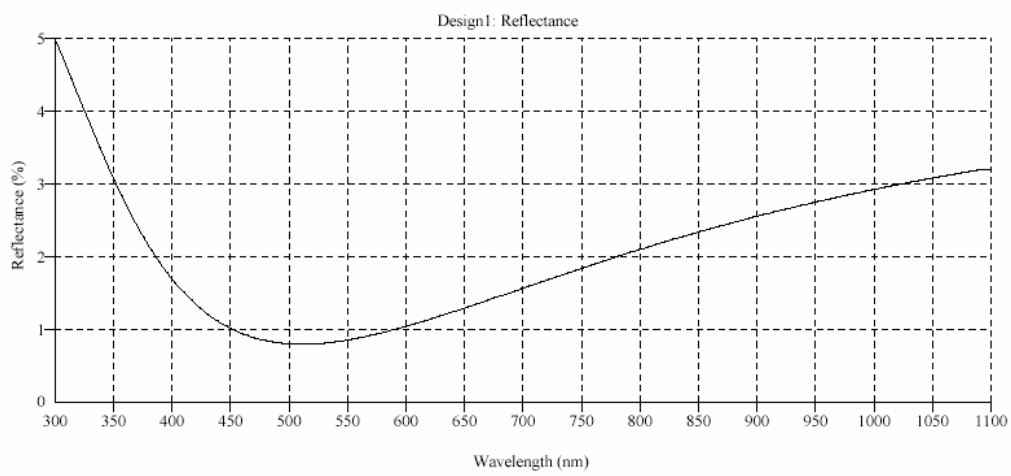

FIGURE 5.9. Reflectance of quarterwave magnesium fluoride layer on OHARA_PBM18Y Glass.

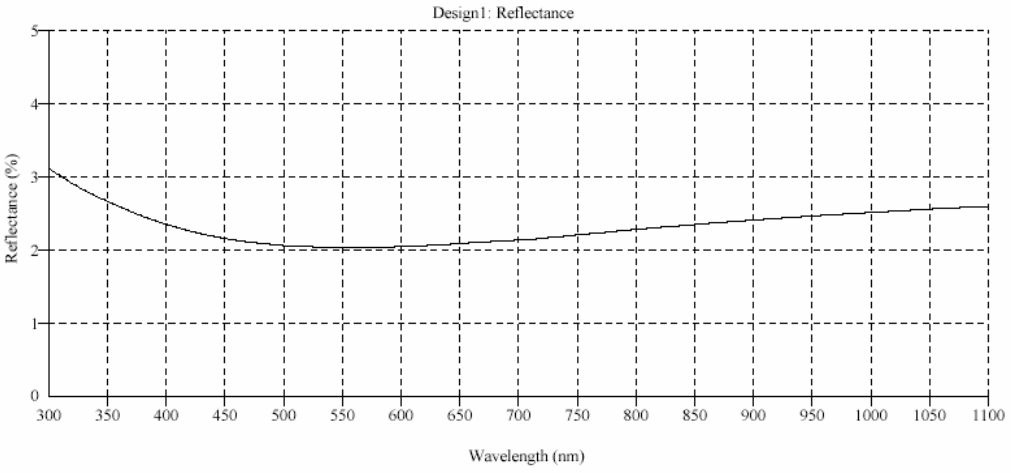

FIGURE 5.10. Reflectance of quarterwave magnesium fluoride layer on optical calcium fluoride.

Chapter 6

CONCLUSION AND FUTURE WORK

6.1 Discussion

6.1.1 Coping with Different Support Processes from Different Manufacturers

6.1.2 Analog versus Digital Dipping Process Control

6.2 Future Work

6.2.1 Enamel-based Moisture Barriers

6.2.2 Deposition of a Hard PVD Layer atop Solgel

6.2.3 The Chupacabra® Hybrid AOTF System

6.3 Conclusions

□

References

[1] J.C. Dainty (ed): Laser Speckle and Related Phenomena, 2nd. ed., Topics Applied Physics Vol. 9 (Springer, Berlin, Heidelberg, New York 1982).

[2] Jill Bechtold: "NSF Proposal for Funds to Build the MAESTRO Spectrograph" (1995).

[3] S. Barraza-Felix: "Regularization of the image division approach to blind deconvolution", OSC Dissertation, University of Arizona (2002).

[4] D. Fabricant, B. McLeod and S. West: "Optical Specifications for the MMT Conversion", version 7, University of Arizona (1999).

[5] Max Born and Emil Wolf: Principles of Optics, sixth corrected edition, Pergamon Press, Oxford (1993).

[6] Eugene Hecht: Optics, second edition, with contributions from Alfred Zajac, Addison-Wesley Publishing Company, Massachussets (1990).

[7] James M. Palmer: The Art of Radiometry, working manuscript (1996).

[8] J. W. Goodman: Introduction to Fourier Optics, McGraw-Hill.

[9] James Stilburn: "Solgel Optical Coating Application", Herzberg Institute of Astrophysics, private commmunication (2001).

[10] H. Angus Macleod: Thin Film Optical Filters, Third Edition, Institute of Physics Publishing, Bristol (2000).

[11] H. Angus Macleod: "Introduction to Thin Film Optical Coatings and Filters", OPTI 412 Class Notes, OSC, University of Arizona (1994).

[12] J. W. Goodman: Statistical Optics, (John Wiley & Sons 1985).

[13] "Parylene Specifications and Properties", Electronic brochure published by the Specialty Coating Systems company, Indianapolis (2000), www.scscookson.com.

[14] Joss Hawthorn, "The Application of broadband AR-coatings extending from the optical to the near-IR", AAO (1999).

[15] S. F. Rosenstiel, I. L. Denry, W. Zhu, P. K. Gupta and R. A. Van der Sluys: "Fluoroalkylethyl silane coating as a moisture barrier for dental ceramics", Technical Note, Journal of Biomedical Materials Research, vol.27, pp.415-417, John Wiley & Sons (1993).

[16] "Performance Property Guide for Dielectric, Optical, Thermal and Mechanical Applications", www.gelest.com (2002).

[17] "Cary 100/300/400/500 Spectrophotometer specifications brochure", Varian, Inc., Palo Alto, www.varianinc.com (2002).

[18] ZC & R Corporation, Private Communication, www.zcrcoatings.com (2003).

[19] "Steward Observatory-90 inch Prime Focus Wide-Field Imager", University of Arizona, http://compton.as.arizona.edu/90prime/index.shtml (2002).